Made available for a limited time for personal research and study only License.

Violating Kirchhoff's Law of Thermal Radiation in Semitransparent Structures

Yubin Park,* Viktar S. Asadchy, Bo Zhao, Cheng Guo, Jiahui Wang, and Shanhui Fan*
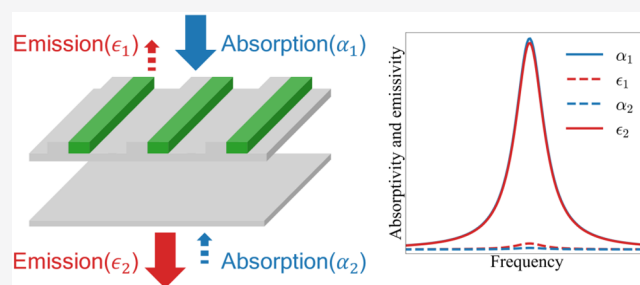
Read Online

ACCESS | Metrics & More | Article Recommendations

ABSTRACT: Kirchhoff's law of thermal radiation imposes a constraint on photon-based energy harvesting processes since part of the incident energy flux is inevitably emitted back to the source. By breaking the reciprocity of the system, it is possible to overcome this restriction and improve the efficiency of energy harvesting. Here, we design and analyze a semitransparent emitter that fully absorbs normally incident energy from a given direction with zero backward and unity forward emissivity. The nearly ideal performance with wavelength-scale thickness is achieved due to the magneto-optical effect and the guided-mode resonance engineered in the emitter structure. We derive the general requirements for the nonreciprocal emitter using the temporal coupled mode theory and the symmetry considerations. Finally, we provide a realistic emitter design based on a photonic crystal slab consisting of a magnetic Weyl semimetal and silicon.

KEYWORDS: *Kirchhoff's law, nonreciprocity, energy harvesting, magneto-optical, photonic crystal, coupled mode theory*

Emission(ϵ_1) Absorption(α_1)
Emission(ϵ_2) Absorption(α_2)
Absorptivity and emissivity — Frequency — α_1, ϵ_1, α_2, ϵ_2

Kirchhoff's law of thermal radiation states that emissivity of a body has to be equal to its absorptivity for a given angle-polarization and frequency of thermal electromagnetic radiation.[1−4] Due to this balance between emission and absorption, whenever an object absorbs light, it must emit energy back to the original source, as illustrated in Figure 1a. Processes of energy harvesting from thermal radiation inevitably suffer from this loss. Thus, overcoming this restriction by violating the Kirchhoff's law is of fundamental importance in order to provide opportunities for higher energy harvesting efficiency.[5]

The Kirchhoff's law is generally obeyed by any system that satisfies the Lorentz reciprocity.[6,7] Once the reciprocity of a system is broken, this law does not hold anymore, and it is possible to achieve a nonreciprocal thermal emitter that exhibits a contrast between the emissivity and the absorptivity.[8−11] Employing the magneto-optical effect is a widely used method to design a nonreciprocal system, and there have been several preceding works exploiting this effect to construct nonreciprocal thermal emitters.[12−16] Zhu and Fan proposed a specific design for a thermal emitter using magneto-optical photonic crystals in ref 12, and Zhao et al. developed this work further by greatly reducing the required magnetic field in the structure in ref 13. In addition, various materials have been studied for the purpose of achieving nonreciprocal thermal emitters.[14−16] All these emitters are opaque and suitable only for reflection-based nonreciprocal systems[5] (see Figure 1b). However, for certain applications it is preferable to have nonreciprocal emission in a transmission-based configuration,

as depicted in Figure 1c. For example, in multijunction solar cells, the *p−n* junctions with higher bandgaps are arranged toward the top of the solar cell. In this case, the emission from the junctions toward the sun represents an intrinsic photon loss mechanism. This loss channel can be avoided if the junctions are made nonreciprocal such that the emitted photons from the upper junctions can be absorbed by the lower-bandgap junctions below to contribute to electrical energy generation (see Figure 1d).

In this paper, we analyze and propose a semitransparent photonic crystal slab that can achieve the above-mentioned functionality, having the total thickness of the order of the operational wavelength. The emitter operates for normal illumination and provides a near-unity difference between the absorptivity and emissivity in the direction of the source as illustrated in Figure 1c.

The paper is organized as follows. First, using the temporal coupled mode theory (CMT), we derive general theoretical conditions required for the violation of Kirchhoff's law in a semitransparent slab for normal incidence. Next, we determine the symmetry of the photonic crystal slab which allows us to
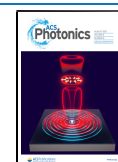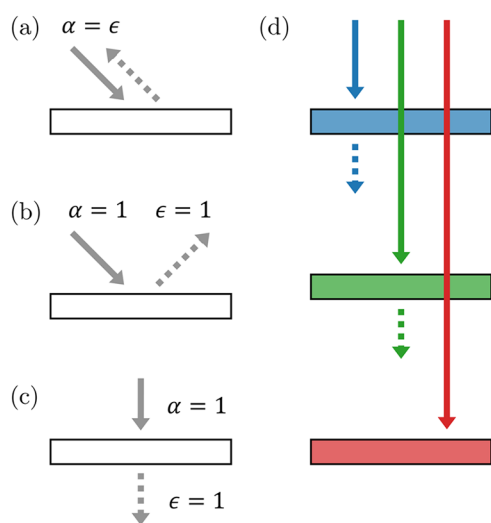
Figure 1. (a–c) Illustrations of the energy flow in various thermal emitter systems: (a) reciprocal case, (b) nonreciprocal opaque case in reflective configuration, and (c) nonreciprocal semitransparent case in transmissive configuration. The arrows define the directions of energy exchange between the emitter and the environment for a given frequency (solid arrows: absorption; dotted arrows: emission). Here, α and ϵ represent the absorptivity and emissivity of the emitter, respectively. (d) Illustration of a multijunction solar cell with the desired nonreciprocal functionality. Each box represents a cell with a particular bandgap. The bandgap of each cell decreases from the top to bottom as expressed with blue, green, and red colors. Each colored arrow indicates the light at the corresponding frequency of the cell bandgap.

obtain the desired thermal performance and provide a possible unit-cell topology based on the guided-mode resonance. This part is followed by the full-wave simulation results of the structure and the qualitative analytical description of its response. Finally, we provide a feasible realization of the photonic crystal slab based on a magnetic Weyl semimetal.

■ THEORY

Energy Balance in Thermal Equilibrium. We start by considering the energy flow in the system shown in Figure 2a.
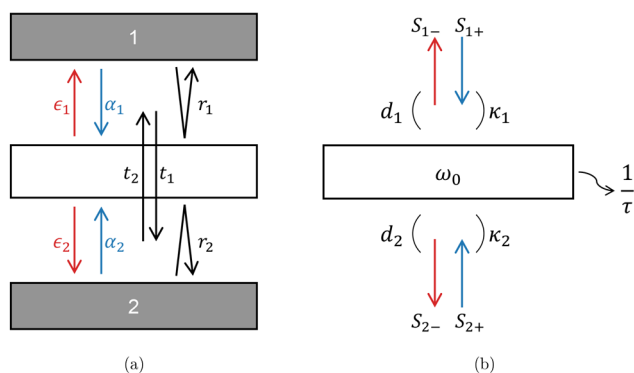

Figure 2. Schematic illustration of the structure. (a) Energy flow diagram of the considered system with radiation channels above and below an emitter. Each arrow represents a route that an energy flow can take. Blackbodies 1 and 2 are at the same temperature as the emitter in the middle. (b) Diagram for CMT analysis. The emitter is expressed as a resonator in the middle.

A nonreciprocal emitter (shown as a white box) is located between blackbodies 1 and 2. Under the thermal equilibrium, there are several constraints imposed on the energy flows (shown with arrows in the figure) in the system which we discuss below. Once the constraints are derived, one can apply them to the nonequilibrium situations. In the figure, $\alpha_{1,2}$ represents the absorptivity of the emitter, which accounts for the ratio of energy absorbed by the emitter to the incoming energy for a given illumination direction. Emissivity of the emitter ϵ_1 (ϵ_2) accounts for the ratio of energy emitted by the emitter toward blackbody 1 (blackbody 2) to the energy emitted by a blackbody emitter in the same situation. Quantities $r_{1,2}$ and $t_{1,2}$ represent the reflectivity and transmissivity, respectively.

Considering first the energy emitted from the blackbody 1 toward the emitter, this energy can take three different routes, as shown in Figure 2a: it can be absorbed by the emitter (α_1), it can be reflected back to the blackbody 1 (r_1), or it can transmit through the emitter (t_1). Thus, the following energy-balance equation has to hold:

$$\alpha_1 + t_1 + r_1 = 1 \tag{1}$$

Similarly, considering the energy absorbed by the blackbody 1, this energy consists of three different components: energy emitted from the emitter (ϵ_1), energy that was reflected at the top (r_1), and energy that transmitted through the emitter upward (t_2). Therefore, another energy-balance equation holds:

$$\epsilon_1 + t_2 + r_1 = 1 \tag{2}$$

Similar equations can be derived from the blackbody 2 side as well:

$$\alpha_2 + t_2 + r_2 = 1 \tag{3}$$

$$\epsilon_2 + t_1 + r_2 = 1 \tag{4}$$

The goal of this work is to design such an emitter which provides full energy absorption from the top half-space (emitted by blackbody 1) with energy emission exclusively toward the bottom half-space (toward blackbody 2). This can be translated into the conditions of $\alpha_1 = 1$ and $\epsilon_1 = 0$, which together with eqs 1−4 provide us with the requirements:

$$\epsilon_1 = \alpha_2 = t_1 = r_1 = r_2 = 0 \tag{5}$$

$$\alpha_1 = \epsilon_2 = t_2 = 1 \tag{6}$$

In other words, under the ideal operation, the emitter will fully absorb energy incident from the top, emit it completely to the bottom, while passing all the energy coming from the bottom without reflection or absorption. We can see from eqs 1 and 2 that, in this design, the absorptivity−emissivity contrast $|\alpha_1 - \epsilon_1|$ is equal to the contrast of transmissivities $|t_1 - t_2|$. This is in sharp contrast with previous designs in refs 5, 12−16, where the absorptivity−emissivity contrast arises from the contrast of reflectivities.

Temporal Coupled Mode Theory Analysis. To achieve the absorptivity−emissivity contrast as discussed above, we consider a resonator system, as shown in Figure 2b. The resonator system couples to two ports on either side of the resonator (one port on each side). We apply CMT here, which is valid when the Q-factor of the resonance is sufficiently high, and we assume a single mode resonance. According to the CMT formalism, our two-port system can be described by the following equations:[17,18]

$$\frac{du}{dt} = \left(j\omega_0 - \gamma - \frac{1}{\tau}\right)u + (\kappa_1 \ \kappa_2)\begin{pmatrix} s_{1+} \\ s_{2+} \end{pmatrix} \quad (7a)$$

$$\begin{pmatrix} s_{1-} \\ s_{2-} \end{pmatrix} = C\begin{pmatrix} s_{1+} \\ s_{2+} \end{pmatrix} + \begin{pmatrix} d_1 \\ d_2 \end{pmatrix}u \quad (7b)$$

where u is the amplitude of the resonant mode normalized so that $|u|^2$ corresponds to the energy, ω_0 is the resonant angular frequency, and γ and $1/\tau$ are the decay rates due to radiation and the material loss, respectively. s_{i+} and s_{i-} are incoming and outgoing wave amplitudes ($i = 1$ for the top port and $i = 2$ for the bottom port), respectively. κ_i and d_i are coupling coefficients to each port, κ_i for absorption and d_i for emission.

$$C = \begin{pmatrix} r_{11} & t_{12} \\ t_{21} & r_{22} \end{pmatrix}$$

is the matrix describing the background scattering process.[19] If we neglect the material loss for now, that is, $1/\tau = 0$, the system is energy-conserving and the parameters satisfy the following equations:[20,21]

$$C^\dagger C = I \quad (8a)$$

$$C\begin{pmatrix} \kappa_1^* \\ \kappa_2^* \end{pmatrix} + \begin{pmatrix} d_1 \\ d_2 \end{pmatrix} = 0 \quad (8b)$$

$$|\kappa_1|^2 + |\kappa_2|^2 = |d_1|^2 + |d_2|^2 = 2\gamma \quad (8c)$$

Note that eq 8 only assumes energy conservation, and no constraint regarding reciprocity is imposed here. Therefore, this holds for our nonreciprocal structure as well.

Then, by adding $1/\tau$ back into eq 7, we can introduce the scattering matrix S as $s_- = S \cdot s_+$, which is given by

$$S = C + \frac{\mathbf{d} \cdot \boldsymbol{\kappa}^T}{j(\omega - \omega_0) + \gamma + 1/\tau} \quad (9)$$

where $\mathbf{s}_\pm = \begin{pmatrix} s_{1\pm} \\ s_{2\pm} \end{pmatrix}$, $\mathbf{d} = \begin{pmatrix} d_1 \\ d_2 \end{pmatrix}$, and $\boldsymbol{\kappa} = \begin{pmatrix} \kappa_1 \\ \kappa_2 \end{pmatrix}$. We note that, in order to take account of material loss by simply adding $1/\tau$ back, we have to assume that the influence on other parameters due to this addition is negligible. This is a common approximation when applying CMT to describe lossy resonator structures.[22] As will be shown below, this approximation works well for the present case.

By comparing the scattering matrix S and the energy flow diagram of Figure 2a, we can deduce the following relations: $|S_{11}|^2 = r_1$, $|S_{21}|^2 = t_1$, $|S_{22}|^2 = r_2$, and $|S_{12}|^2 = t_2$. Therefore, expressions for absorptivities and emissivities can be derived using eq 8:

$$\alpha_1(\omega) = 1 - |S_{11}|^2 - |S_{21}|^2 = \frac{2}{\tau}\frac{|\kappa_1|^2}{(\omega - \omega_0)^2 + (\gamma + 1/\tau)^2} \quad (10a)$$

$$\epsilon_1(\omega) = 1 - |S_{11}|^2 - |S_{12}|^2 = \frac{2}{\tau}\frac{|d_1|^2}{(\omega - \omega_0)^2 + (\gamma + 1/\tau)^2} \quad (10b)$$

$$\alpha_2(\omega) = 1 - |S_{22}|^2 - |S_{12}|^2 = \frac{2}{\tau}\frac{|\kappa_2|^2}{(\omega - \omega_0)^2 + (\gamma + 1/\tau)^2} \quad (10c)$$

$$\epsilon_2(\omega) = 1 - |S_{22}|^2 - |S_{21}|^2 = \frac{2}{\tau}\frac{|d_2|^2}{(\omega - \omega_0)^2 + (\gamma + 1/\tau)^2} \quad (10d)$$

Note that these are Lorentzian functions and, as will be shown below, they accurately describe the actual spectra near the resonance frequency for the photonic crystal slab. Note also that α_i is proportional to $|\kappa_i|^2$ and ϵ_i is proportional to $|d_i|^2$ (for $i = 1$ and 2). This accords with our initial setup of CMT, where κ_i is the in-coupling coefficient and d_i is the out-coupling coefficient between the port and the resonator.

Since our goal is to maximize the contrast between absorptivity and emissivity, we now look at the expression for $|\alpha_1 - \epsilon_1|$ at resonance frequency $\omega = \omega_0$:

$$|\alpha_1(\omega_0) - \epsilon_1(\omega_0)| = \left|\frac{|\kappa_1|^2}{2\gamma} - \frac{|d_1|^2}{2\gamma}\right|\frac{4\gamma\frac{1}{\tau}}{\left(\gamma + \frac{1}{\tau}\right)^2} \quad (11)$$

It is clear from eq 11 that maximization of $|\alpha_1(\omega_0) - \epsilon_1(\omega_0)|$ can be achieved by satisfying two separate conditions. The first condition is maximizing the difference between the normalized coupling rates $\frac{|\kappa_1|^2}{2\gamma}$ and $\frac{|d_1|^2}{2\gamma}$. The second condition is the critical coupling condition of $\gamma = 1/\tau$, which was also pointed out in ref 12. Thus, a proper design requires simultaneous maximization of the magnitude difference between the input and the output coupling coefficients and matching of the radiation and absorption losses.

◾ DESIGN

Based on the CMT formalism presented in the previous section, we consider an emitter consisting of a photonic crystal structure shown in Figure 3. We place two bars, made of dielectric and magneto-optical materials, on top of a dielectric slab as shown at the top of Figure 3. In addition, we place another parallel dielectric slab at a distance l away in the x
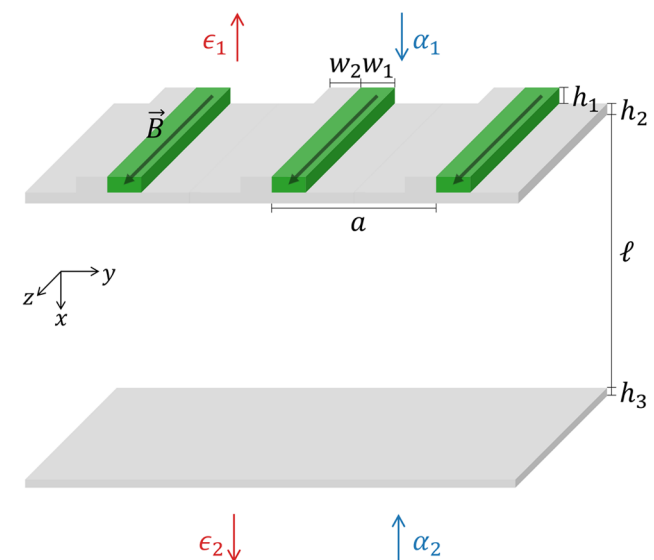

Figure 3. Geometry of the designed nonreciprocal thermal emitter that breaks the Kirchhoff's law. The gray regions represent dielectric, while the green regions represent magneto-optical material with magnetization in the z direction. Two infinitely long bars are located on top of a slab, and another parallel slab is located at a distance l away. Wave propagation is along the $\pm x$ direction.

direction, as shown at the bottom of the figure. The entire structure is surrounded by air. In this work, we choose the dielectric material to be silicon in order to exploit the strong index contrast between silicon and air. The magnetization direction in the magneto-optical regions is parallel to the z axis, and we express the permittivity of the magneto-optical material by a tensor

$$\overline{\overline{\varepsilon}} = \begin{bmatrix} \varepsilon_d & -j\varepsilon_a & 0 \\ j\varepsilon_a & \varepsilon_d & 0 \\ 0 & 0 & \varepsilon_z \end{bmatrix} \tag{12}$$

Let us decompose the diagonal component into real and imaginary parts so that $\varepsilon_d = \varepsilon_{dr} - j\varepsilon_{di}$. The imaginary part accounts for the material loss. The off-diagonal component ε_a characterizes the strength of the nonreciprocal effect and arises from the magnetization of the material. In most situations, the imaginary part of ε_a is very small and can be neglected. For incident light, we consider a TM-polarized wave propagating in the $\pm x$ direction with a magnetic field in the z direction and an electric field in the xy plane. The setup, therefore, is in the Voigt configuration, with the wave propagating perpendicular to the direction of magnetization.

As shown above based on eqs 1 and 2, maximization of the contrast between α_1 and ϵ_1 has the same conditions as maximization of the contrast between the transmission along the two directions. Therefore, the design of nonreciprocal emitters is connected with isolator designs that seek to maximize the transmission contrast. On the other hand, since our motivation is to construct such a nonreciprocal device in the context of energy harvesting, the device needs to operate in the optical or thermal frequency range for broad-area incident light. Thus, many standard designs of isolators are not applicable. For example, microwave isolators[23,24] are not appropriate due to low-frequency operation, while optical implementations based on waveguide geometries[25,26] do not operate with free-space light illuminations. Moreover, those existing optical isolator designs that operate for free-space broad-area incident light at the optical frequencies also have limitations for our purpose. The isolators based on the Faraday configuration[27] are generally bulky and additionally require polarizers and antireflective coatings, resulting in the final structure with a large thickness. In the Voigt configuration,[28] most isolators operate either only in the reflection regime or only for the oblique illuminations.[29,30] Thus, the challenge for a compact nonreciprocal thermal emitter operating in transmission has not been addressed in previous works.

In order to achieve nonreciprocal emission (or isolation in transmission), the magnetic symmetry group of the structure must exclude some of the symmetry operations.[31,32] For the normal incidence in the $\pm x$ direction, the representing examples of the symmetries that simultaneously need to be broken are R, I, m_x, m_y', m_z', n_x', p_y, and p_z. Here, R represents the time-reversal symmetry operation, and I represents the inversion symmetry operation. m_j represents the mirror symmetry with respect to the plane perpendicular to the j axis, while n_j and p_j represent the n-fold and p-fold rotation symmetry, respectively, about the j axis, where n is any natural number higher than 1 and p is any even natural number. Index j can be any one of x, y, and z, while $'$ means an additional time-reversal operation to the preceding operation (e.g., $m_j' = m_j \odot R$). Considering only the array of bars in Figure 3

(excluding both continuous slabs), we can see that their symmetry group includes only the symmetry operations m_x', m_z, and $2_y'$, which does not preclude the nonreciprocal emission. Therefore, the array of bars consisting of dielectric and magneto-optical materials (with the given magnetization direction) by itself can exhibit the desired nonreciprocal property. However, the nonreciprocal effect in such a system is generally weak due to its low Q-factor. Hence, we add two continuous slabs: the upper one for creating a strong guided-mode resonance response[19] and the bottom one, placed sufficiently far apart, for independent tuning of the background scattering matrix C in our CMT model without affecting the total line width and the resonant frequency. The bottom slab provides us with an additional degree of freedom useful for simplifying the design. The only symmetry present in the final system in Figure 3 is m_z, which satisfies the symmetry requirement as discussed above.

In the structure of Figure 3, for TM-polarized light normally incident onto the structure, the part of the scattered field that arises from the magneto-optical materials has the same pattern independent whether the light is incident from the top or the bottom. Moreover, the scattered field above or below the structure exhibits a 180° phase difference. The dielectric structures surrounding the magneto-optical materials have the right symmetry to ensure that such scattered field can radiate into the far field. Consequently, there is constructive or destructive interference depending on the direction of incident light, which results in the transmission contrast.

■ RESULTS AND DISCUSSION

Optimization for Ideal Performance. Here, we explain the optimization of our design with the guidance of the CMT model developed above. First, to illustrate the general principles, we conduct the optimization without restricting ourselves to any specific materials. Then, in the following section, we discuss more about the material constraints.

We conduct full-wave simulations of the emitter shown in Figure 3 using a 2D finite-element frequency domain solver (RF module in COMSOL Multiphysics). A periodic boundary condition is applied in the xy plane. We compute the spectra of reflectivities and transmissivities as we illuminate the non-reciprocal structure by TM-polarized light along either the $+x$ or $-x$ direction (see Figure 3). We calculate, using eq 10, the spectra of absorptivities and emissivities from the reflectivities and transmissivities.

In the simulations, we optimize the structural parameters of the emitter subject to the following material properties. For the dielectric regions, we set the dielectric constant to $\varepsilon_s = 12$, which approximately corresponds to that of silicon in the infrared frequency range. For the magneto-optical material, we choose the real part of the diagonal relative permittivity to be $\varepsilon_{dr} = 6.25$. This corresponds to that of bismuth iron garnet (BIG), also in the infrared frequency range, which has been a widely used material for magneto-optical applications in several preceding studies.[29,33−35] Under these constraints, we first tune the geometrical parameters, that is, w_1, w_2, h_1, h_2, h_3, and l, shown in Figure 3, as well as the off-diagonal relative permittivity ε_a, so that we can maximize $\left| \frac{|\kappa_1|^2}{2\gamma} - \frac{|d_1|^2}{2\gamma} \right|$ in eq 11. Here, we choose the periodicity of our structure subwavelength so that no diffraction harmonics are excited. In this process, we fit the absorptivity and emissivity spectra obtained from the simulation to the expressions derived from
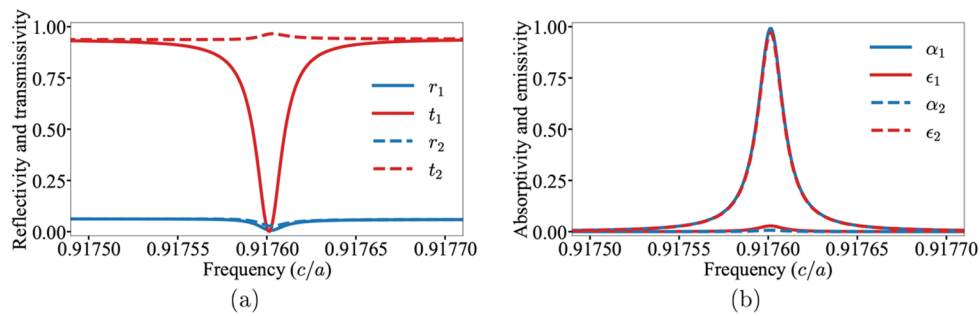
Figure 4. Response functions of the optimized nonreciprocal emitter with nearly ideal performance. The shown results are for the TM-polarized light: (a) reflectivities and transmissivities; (b) absorptivities and emissivities.

our CMT model (eq 10), to determine κ_i, d_i, and γ. Once the contrast close to unity is achieved, we then tune the imaginary part of the diagonal relative permittivity ε_{di} to satisfy the critical coupling condition. Since $1/\tau$, which is also determined from the fitting, can be controlled independently from other CMT parameters by varying ε_{di}, we can safely tune the material loss at the end without affecting the parameters determined in the previous step.

As a result of optimization, $\varepsilon_a = 0.19$ and $\varepsilon_{di} = 0.0015$ are chosen. These values are approximately 3× larger and 60× smaller than the actual values for BIG, respectively. The optimized geometric parameters read as $w_1 = 0.21a$, $w_2 = 0.19a$, $h_1 = 0.097a$, $h_2 = 0.065a$, $h_3 = 0.05a$, and $l = 1.67a$, where a is the periodicity. All the geometric parameters are illustrated in Figure 3 with the correct scaling.

Figure 4 shows the response functions for the optimized emitter. As one can see, a nearly complete contrast between the absorptivity and emissivity is achieved, that is, $|\alpha_1(\omega_0) - \epsilon_1(\omega_0)| = 0.965$. At the resonance, the reflectivities are negligible, so that absorptivity-emissivity contrast comes from the transmissivity contrast. We note that our design procedure is general and can be applied to arbitrary frequencies by tuning the material and structural properties.

As we can see from eq 11, a key consideration for achieving high contrast between the absorptivity and the emissivity is to achieve a large difference between the in-coupling coefficient κ_1 and out-coupling coefficient d_1. Therefore, below we examine the influence of the magneto-optical effect on such coupling constants by considering the dependency of the normalized coupling rates $\frac{|\kappa_1|^2}{2\gamma}$ and $\frac{|d_1|^2}{2\gamma}$ as functions of ε_a (Figure 5). Note that we tune ε_a in a range where it is sufficiently small to be considered as a perturbation, while maintaining the other parameters as they were determined from the optimization process.

When $\varepsilon_a = 0$, the input and output coupling rates exactly match, and this corresponds to the reciprocal case without magnetization. As ε_a increases, the two coupling rates split and the relation between this splitting and ε_a appears to be linear. This linearity can be explained by applying the first-order perturbation theory[36] to the relation between the coupling rates and the Hamiltonian of the system and by considering a time-reversal conjugate system. The out-coupling rate from a resonator to an adjacent port has the following relation to Hamiltonian V:[37]

$$|d_1|^2 \propto \overline{|\langle c|V|q\rangle|^2}\, g(\omega) \tag{13}$$
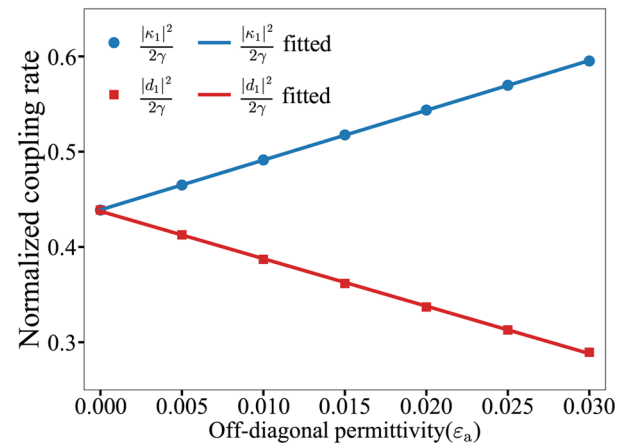

Figure 5. Normalized coupling rates vs the off-diagonal permittivity. For small values of ε_a, the splitting of the input and output coupling rates is linear. The geometrical parameters of the structure are determined from the optimization process.

where $|q\rangle$ and $|c\rangle$ represent a state in the port and the resonator, respectively, V is the Hamiltonian that describes the coupling between the port and the resonator, the overline denotes the average over the states in the port, and g is the density of states in the port. Then, if we consider small ε_a as a perturbation applied to the original system, the following approximation holds:

$$\Delta|d_1|^2 \propto \overline{|\langle c|V + \delta V|q\rangle|^2} - \overline{|\langle c|V|q\rangle|^2}$$

$$\approx \overline{\langle q|V|c\rangle\langle c|\delta V|q\rangle + \langle c|V|q\rangle\langle q|\delta V|c\rangle} \tag{14}$$

where δV is the perturbation of the Hamiltonian coming from the addition of ε_a. Therefore, when ε_a is sufficiently small, a change in the out-coupling rate $\Delta|d_1|^2$ is linearly proportional to ε_a due to eqs 13 and 14 since the Hamiltonian elements $\langle c|\delta V|q\rangle$ and $\langle q|\delta V|c\rangle$ are linear with respect to ε_a. Meanwhile, the in-coupling coefficient κ_1 in the emitter corresponds to the out-coupling coefficient $\tilde{d}_1$ in its time-reversal conjugate system[21] (tilde symbol denotes the conjugation operator) since these coefficients can be determined in the corresponding lossless system, as we discussed in the CMT analysis section. Then, since the conjugate emitter has the off-diagonal permittivity ε_a with the opposite sign, the slope of $\Delta|\tilde{d}_1|^2 = \Delta|\kappa_1|^2$ will be opposite to that of $\Delta|d_1|^2$. This behavior leads to the linear and opposite splitting of the coupling rates $|d_1|^2$ and $|\kappa_1|^2$. On the other hand, if we consider $\tilde{\gamma}$ in the conjugate system, due to eq 8c and the relationship between the coupling coefficients of the original and conjugate systems ($\tilde{d}_i = \kappa_i$ and $\tilde{\kappa}_i$
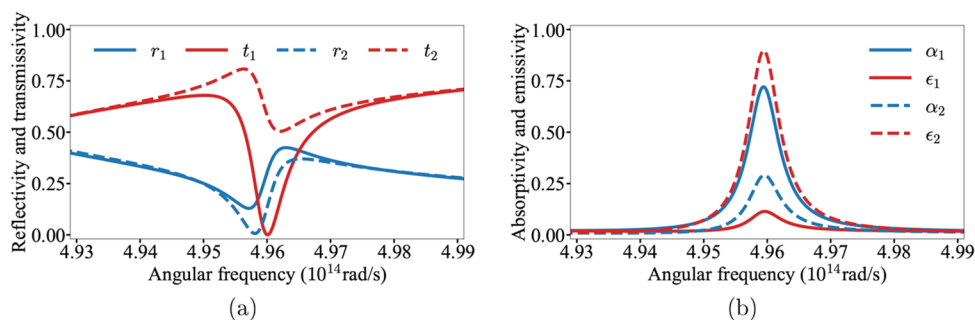
Figure 6. Response functions of the optimized emitter consisting of Weyl semimetal and silicon. The shown results are for the TM-polarized light: (a) reflectivities and transmissivities; (b) absorptivities and emissivities.

$= d_i$ for $i = 1$ and 2), $\tilde{\gamma}$ has to be equal to γ of the original system. As a result, γ is an even function with respect to ε_a and constant in the first-order approximation. Thus, the normalized coupling rates $\frac{|d_1|^2}{2\gamma}$ and $\frac{|\kappa_1|^2}{2\gamma}$, shown in Figure 5, also vary linearly with respect to ε_a, with different slope signs. Note that this linear and monotonic increase of splitting is limited to the regime where ε_a is sufficiently small, and a similar behavior is not assured when the first order approximation does not hold anymore.

Emitter Realization Based on Weyl Semimetal. Although the results shown above demonstrate nearly perfect nonreciprocal emitter performance, finding magneto-optical material whose permittivity is equal to the optimized one can be a nontrivial task. For example, BIG with realistic losses in the diagonal permittivity and realistic ε_a will not provide a high emissivity-absorptivity contrast. As a rule of thumb, the high contrast requires sufficiently small ε_{di} and sufficiently large ε_a of the magneto-optical material. Here, we propose to use a magnetic Weyl semimetal of EuCd$_2$As$_2$ as one candidate of the magneto-optical material with such desired properties.

We use the permittivity dispersion data from refs 30, 38, and 39. While this material is relatively lossy, it has an extremely high off-diagonal permittivity, which makes its overall performance good. Since ε_a is large enough at most frequencies, we consider the operating frequency that minimizes the $\varepsilon_{di}/\varepsilon_{dr}$ value. At frequency $\omega_0 = 4.96 \times 10^{14}$ rad/s, the permittivity values for the Weyl semimetal are $\varepsilon_d = 3.47 - j0.0733$ and $\varepsilon_a = -2.39$. Since the operating frequency is fixed now, we set ε_s to 11.7, which corresponds to the dielectric constant of silicon at this frequency. Next, using the approach described above we optimize the geometry of the Weyl emitter at the resonance frequency ω_0. The optimized geometric parameters read as $a = 1.61\ \mu$m, $w_1 = 400$ nm, $w_2 = 220$ nm, $h_1 = 830$ nm, $h_2 = 700$ nm, $h_3 = 80$ nm, and $l = 2.13\ \mu$m. We note that the bandwidth of the resonance is about 10^{12} rad/s, which is narrow enough to neglect the impact of dispersion, and we assume constant permittivity values throughout this resonance regime.

As can be seen from Figure 6a, the asymmetric Fano line shape of the guided-mode resonance appears in the reflectivity and transmissivity spectra. At this resonance, the absorptivity-emissivity contrast reaches $|\alpha_1(\omega_0) - \epsilon_1(\omega_0)| \approx 0.6$ (see Figure 6b). Therefore, relatively high contrast in absorptivity and emissivity can be achieved with realistic material systems. Importantly, the operating frequency of the nonreciprocal emitter can be shifted by changing the Fermi level of the Weyl semimetal.[30,38]

Note that when considering the electromagnetic properties of a Weyl semimetal, it is important to take account of the Fermi-arc surface states that can affect the boundary conditions for the electromagnetic waves.[40] However, in our simulation, the magnitude of the tangential electric and magnetic fields along the boundary of the Weyl semimetal region turns out to meet the condition of neglecting the Fermi-arcs ($\frac{e^2}{h}\frac{|E_t|}{|H_z|} \ll 1$, where E_t is the tangential electric field and H_z is the magnetic field in the z direction) proposed in ref 30. Thus, we ignore this effect and consider the conventional boundary conditions.

■ CONCLUSION

In conclusion, we show that it is possible to violate the Kirchhoff's law of radiation in a semitransparent structure. We develop a CMT framework to guide the design of a nonreciprocal thermal emitter that fully absorbs normally incident energy from a given direction with zero backward but unity forward emissivity. Unlike previous reflection-based designs, we suppress reflections and acquire absorptivity-emissivity contrast from difference in transmissivities for each illumination direction. Exploiting the guided-mode resonance, we obtain nearly ideal performance for the emitter, which has a thickness of 1.7× the operating wavelength. In addition, we demonstrate that the normalized coupling rates in the CMT model are linear functions of the magneto-optical off-diagonal permittivity in the small perturbation limit. We also show that, taking into account limited permittivity spectrum of natural materials, it is still possible to reach a significant contrast between the emissivity and absorptivity using recently discovered magnetic Weyl semimetal of EuCd$_2$As$_2$. When applied to multijunction solar cells, our semitransparent structure will allow the reuse of light energy that would be wasted otherwise. Furthermore, directional transmission in our structure coincides with the function of nonreciprocal isolators. Thus, our work may serve as a stepping stone for further utilization of nonreciprocal systems in novel energy harvesting devices and optical isolators.

■ AUTHOR INFORMATION

Corresponding Authors

Yubin Park − *Department of Electrical Engineering, Stanford University, Stanford, California 94305, United States;* ● orcid.org/0000-0001-9734-5977; Email: yubinpark@stanford.edu

Shanhui Fan − *Department of Electrical Engineering, Stanford University, Stanford, California 94305, United States; Ginzton Laboratory, Stanford University, Stanford, California 94305, United States;* ● orcid.org/0000-0002-0081-9732; Email: shanhui@stanford.edu

Authors

Viktar S. Asadchy − *Ginzton Laboratory, Stanford University, Stanford, California 94305, United States;* ⦿ orcid.org/ 0000-0002-9840-4737

Bo Zhao − *Ginzton Laboratory, Stanford University, Stanford, California 94305, United States;* ⦿ orcid.org/0000-0002-3648-6183

Cheng Guo − *Department of Applied Physics, Stanford University, Stanford, California 94305, United States;* ⦿ orcid.org/0000-0003-4913-8150

Jiahui Wang − *Department of Applied Physics, Stanford University, Stanford, California 94305, United States*

Complete contact information is available at:
https://pubs.acs.org/10.1021/acsphotonics.1c00612

Notes

The authors declare no competing financial interest.

■ REFERENCES

(1) Kirchhoff, G. Ueber das Verhältniss zwischen dem Emissionsvermögen und dem Absorptionsvermögen der Körper für Wärme und Licht. *Ann. Phys.* **1860**, *185*, 275−301.

(2) Planck, M. *The Theory of Heat Radiation*, 2nd ed.; P. Blakiston's Son & Co., 1914; pp 22−45.

(3) Howell, J. R.; Mengüc, M. P.; Daun, K.; Siegel, R. *Thermal Radiation Heat Transfer*, 7th ed.; CRC Press, 2021; pp 53−72.

(4) Bergman, T. L.; Lavine, A. S. *Fundamentals of Heat and Mass Transfer*, 8th ed.; John Wiley & Sons, 2017; pp 701−760.

(5) Green, M. A. Time-asymmetric photovoltaics. *Nano Lett.* **2012**, *12*, 5985−5988.

(6) Landau, L. D.; Lifshitz, E. M. *Electrodynamics of Continuous Media*, 2nd ed.; Pergamon Press, 1984; pp 308−310.

(7) Han, S. E. Theory of thermal emission from periodic structures. *Phys. Rev. B: Condens. Matter Mater. Phys.* **2009**, *80*, 155108.

(8) Ries, H. Complete and reversible absorption of radiation. *Appl. Phys. B: Photophys. Laser Chem.* **1983**, *32*, 153−156.

(9) Snyder, W. C.; Wan, Z.; Li, X. Thermodynamic constraints on reflectance reciprocity and Kirchhoff's law. *Appl. Opt.* **1998**, *37*, 3464−3470.

(10) Zhang, Z. M.; Wu, X.; Fu, C. Validity of Kirchhoff's law for semitransparent films made of anisotropic materials. *J. Quant. Spectrosc. Radiat. Transfer* **2020**, *245*, 106904.

(11) Khandekar, C.; Khosravi, F.; Li, Z.; Jacob, Z. New spin-resolved thermal radiation laws for nonreciprocal bianisotropic media. *New J. Phys.* **2020**, *22*, 123005.

(12) Zhu, L.; Fan, S. Near-complete violation of detailed balance in thermal radiation. *Phys. Rev. B: Condens. Matter Mater. Phys.* **2014**, *90*, 220301.

(13) Zhao, B.; Shi, Y.; Wang, J.; Zhao, Z.; Zhao, N.; Fan, S. Near-complete violation of Kirchhoff's law of thermal radiation with a 0.3T magnetic field. *Opt. Lett.* **2019**, *44*, 4203−4206.

(14) Wang, H.; Wu, H.; Shen, Z. Nonreciprocal optical properties of thermal radiation with SiC grating magneto-optical materials. *Opt. Express* **2017**, *25*, 19609−19618.

(15) Wang, H.; Wu, H.; Zhou, J.-q. Nonreciprocal optical properties based on magneto-optical materials: n-InAs, GaAs and HgCdTe. *J. Quant. Spectrosc. Radiat. Transfer* **2018**, *206*, 254−259.

(16) Pajovic, S.; Tsurimaki, Y.; Qian, X.; Chen, G. Intrinsic nonreciprocal reflection and violation of Kirchhoff's law of radiation in planar type-I magnetic Weyl semimetal surfaces. *Phys. Rev. B: Condens. Matter Mater. Phys.* **2020**, *102*, 165417.

(17) Haus, H. A. *Waves and Fields in Optoelectronics*; Prentice-Hall, 1984; pp 197−230.

(18) Fan, S. In *Optical Fiber Telecommunications V A*, 5th ed.; Kaminow, I. P., Li, T., Willner, A. E., Eds.; Optics and Photonics; Academic Press: Burlington, 2008; pp 431−454.

(19) Fan, S.; Suh, W.; Joannopoulos, J. D. Temporal coupled-mode theory for the Fano resonance in optical resonators. *J. Opt. Soc. Am. A* **2003**, *20*, 569−572.

(20) Wang, K. X. Time-reversal symmetry in temporal coupled-mode theory and nonreciprocal device applications. *Opt. Lett.* **2018**, *43*, 5623−5626.

(21) Zhao, Z.; Guo, C.; Fan, S. Connection of temporal coupled-mode-theory formalisms for a resonant optical system and its time-reversal conjugate. *Phys. Rev. A: At., Mol., Opt. Phys.* **2019**, *99*, 033839.

(22) Piper, J. R.; Fan, S. Total absorption in a graphene monolayer in the optical regime by critical coupling with a photonic crystal guided resonance. *ACS Photonics* **2014**, *1*, 347−353.

(23) Pozar, D. M. *Microwave Engineering*, 4th ed.; John Wiley & Sons, 2012; pp 451−493.

(24) Kord, A.; Sounas, D. L.; Alù, A. Microwave nonreciprocity. *Proc. IEEE* **2020**, *108*, 1728−1758.

(25) Dötsch, H.; Bahlmann, N.; Zhuromskyy, O.; Hammer, M.; Wilkens, L.; Gerhardt, R.; Hertel, P.; Popkov, A. F. Applications of magneto-optical waveguides in integrated optics: review. *J. Opt. Soc. Am. B* **2005**, *22*, 240−253.

(26) Williamson, I. A. D.; Minkov, M.; Dutt, A.; Wang, J.; Song, A. Y.; Fan, S. Integrated nonreciprocal photonic devices with dynamic modulation. *Proc. IEEE* **2020**, *108*, 1759−1784.

(27) Saleh, B. E. A.; Teich, M. C. *Fundamentals of Photonics*, 3rd ed.; John Wiley & Sons, 2019; pp 240−243.

(28) Zvezdin, A. K.; Kotov, V. A. *Modern Magnetooptics and Magnetooptical Materials*; IOP Publishing, 1997; Chapter 1.

(29) Yu, Z.; Wang, Z.; Fan, S. One-way total reflection with one-dimensional magneto-optical photonic crystals. *Appl. Phys. Lett.* **2007**, *90*, 121133.

(30) Asadchy, V. S.; Guo, C.; Zhao, B.; Fan, S. Sub-wavelength passive optical isolators using photonic structures based on weyl semimetals. *Adv. Opt. Mater.* **2020**, *8*, 2000100.

(31) Figotin, A.; Vitebsky, I. Nonreciprocal magnetic photonic crystals. *Phys. Rev. E: Stat. Phys., Plasmas, Fluids, Relat. Interdiscip. Top.* **2001**, *63*, 066609.

(32) Guo, C.; Fan, S. Theoretical constraints on reciprocal and non-reciprocal many-body radiative heat transfer. *Phys. Rev. B: Condens. Matter Mater. Phys.* **2020**, *102*, 085401.

(33) Adachi, N.; Denysenkov, V. P.; Khartsev, S. I.; Grishin, A. M.; Okuda, T. Epitaxial Bi3Fe5O12(001) films grown by pulsed laser deposition and reactive ion beam sputtering techniques. *J. Appl. Phys.* **2000**, *88*, 2734−2739.

(34) Tepper, T.; Ross, C. A. Pulsed laser deposition and refractive index measurement of fully substituted bismuth iron garnet films. *J. Cryst. Growth* **2003**, *255*, 324−331.

(35) Wang, Z.; Fan, S. Optical circulators in two-dimensional magneto-optical photonic crystals. *Opt. Lett.* **2005**, *30*, 1989−1991.

(36) Joannopoulos, J. D.; Johnson, S. G.; Winn, J. N.; Meade, R. D. *Photonic Crystals: Molding the Flow of Light*, 2nd ed.; Princeton University Press, 2008; Chapter 2.

(37) Fan, S.; Villeneuve, P. R.; Joannopoulos, J. D.; Khan, M. J.; Manolatou, C.; Haus, H. A. Theoretical analysis of channel drop tunneling processes. *Phys. Rev. B: Condens. Matter Mater. Phys.* **1999**, *59*, 15882−15892.

(38) Zhao, B.; Guo, C.; Garcia, C. A. C.; Narang, P.; Fan, S. Axion-field-enabled nonreciprocal thermal radiation in weyl semimetals. *Nano Lett.* **2020**, *20*, 1923−1927.

(39) Guo, C.; Zhao, B.; Huang, D.; Fan, S. Radiative thermal router based on tunable magnetic weyl semimetals. *ACS Photonics* **2020**, *7*, 3257−3263.

(40) Chen, Q.; Kutayiah, A. R.; Oladyshkin, I.; Tokman, M.; Belyanin, A. Optical properties and electromagnetic modes of Weyl semimetals. *Phys. Rev. B: Condens. Matter Mater. Phys.* **2019**, *99*, 075137.